

# Rational Design of Bisphosphonate Lipid-like Materials for mRNA Delivery to the Bone Microenvironment

Lulu Xue, Ningqiang Gong, Sarah J. Shepherd, Xinhong Xiong, Xueyang Liao, Xuexiang Han, Gan Zhao, Chao Song, Xisha Huang, Hanwen Zhang, Marshall S. Padilla, Jingya Qin, Yi Shi, Mohamad-Gabriel Alameh, Darrin J. Pochan, Karin Wang, Fanxin Long, Drew Weissman, and Michael J. Mitchell\*



Cite This: <https://doi.org/10.1021/jacs.2c02706>



Read Online

ACCESS |



Metrics & More

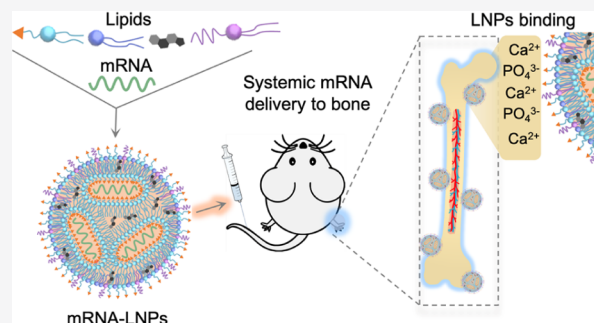


Article Recommendations



Supporting Information

**ABSTRACT:** The development of lipid nanoparticle (LNP) formulations for targeting the bone microenvironment holds significant potential for nucleic acid therapeutic applications including bone regeneration, cancer, and hematopoietic stem cell therapies. However, therapeutic delivery to bone remains a significant challenge due to several biological barriers, such as low blood flow in bone, blood–bone marrow barriers, and low affinity between drugs and bone minerals, which leads to unfavorable therapeutic dosages in the bone microenvironment. Here, we construct a series of bisphosphonate (BP) lipid-like materials possessing a high affinity for bone minerals, as a means to overcome biological barriers to deliver mRNA therapeutics efficiently to the bone microenvironment *in vivo*. Following *in vitro* screening of BP lipid-like materials formulated into LNPs, we identified a lead BP-LNP formulation, 490BP-C14, with enhanced mRNA expression and localization in the bone microenvironment of mice *in vivo* compared to 490-C14 LNPs in the absence of BPs. Moreover, BP-LNPs enhanced mRNA delivery and secretion of therapeutic bone morphogenetic protein-2 from the bone microenvironment upon intravenous administration. These results demonstrate the potential of BP-LNPs for delivery to the bone microenvironment, which could potentially be utilized for a range of mRNA therapeutic applications including regenerative medicine, protein replacement, and gene editing therapies.



## 1. INTRODUCTION

The bone microenvironment is a distinct, highly dynamic region that consists of bone cells, cells of the hematopoietic and immune systems, fibroblasts, stromal cells, and endothelial cells as well as extracellular matrix (ECM) with abundant growth and/or signaling factors.<sup>1–4</sup> These various cell types and ECM proteins enable orchestrated bone remodeling,<sup>5,6</sup> hematopoiesis,<sup>7,8</sup> immune function regulation,<sup>9,10</sup> and tissue regeneration.<sup>11,12</sup> Recently, increased incidences of various skeletal diseases and age-related bone abnormalities, including osteoporosis, osteoarthritis, osteomyelitis, and bone cancer, have inspired the investigation of novel biomaterials for bone microenvironment targeting.<sup>13</sup> However, various characteristics of the bone microenvironment, including reduced blood flow and vascularization compared to other organs, the blood–bone marrow barrier, poorly perfused bone sections, highly dense hierarchic structures, and low affinity between drugs and bone minerals, create several challenges for successful delivery of therapeutics into bone.<sup>10,14,15</sup> Currently, organic/inorganic nanocomposites<sup>15,16</sup> and hydrogels<sup>17,18</sup> have been developed for targeted and local delivery of pharmacological-based therapeutics such as antibiotics,<sup>19,20</sup> growth factors,<sup>21,22</sup> anti-

inflammatory molecules,<sup>23,24</sup> anticancer agents,<sup>25,26</sup> and hormones.<sup>27</sup> However, low delivery efficiency of these materials necessitates high dosing to achieve ideal therapeutic dosage at diseased sites and long-term bioavailability, increasing the incidence of severe side effects. These limitations suggest the need for efficient and safe therapeutic approaches for targeted drug delivery to the bone microenvironment.

One class of therapeutics that are of particular interest for delivery to bone are nucleic acid therapeutics, which regulate therapeutic gene expression within targeted sites to treat diseases by delivering exogenous nucleic acids, such as plasmid DNA (pDNA), small interfering RNA (siRNA), messenger RNA (mRNA), and microRNA (miRNA).<sup>28–32</sup> Currently, the

Received: March 11, 2022

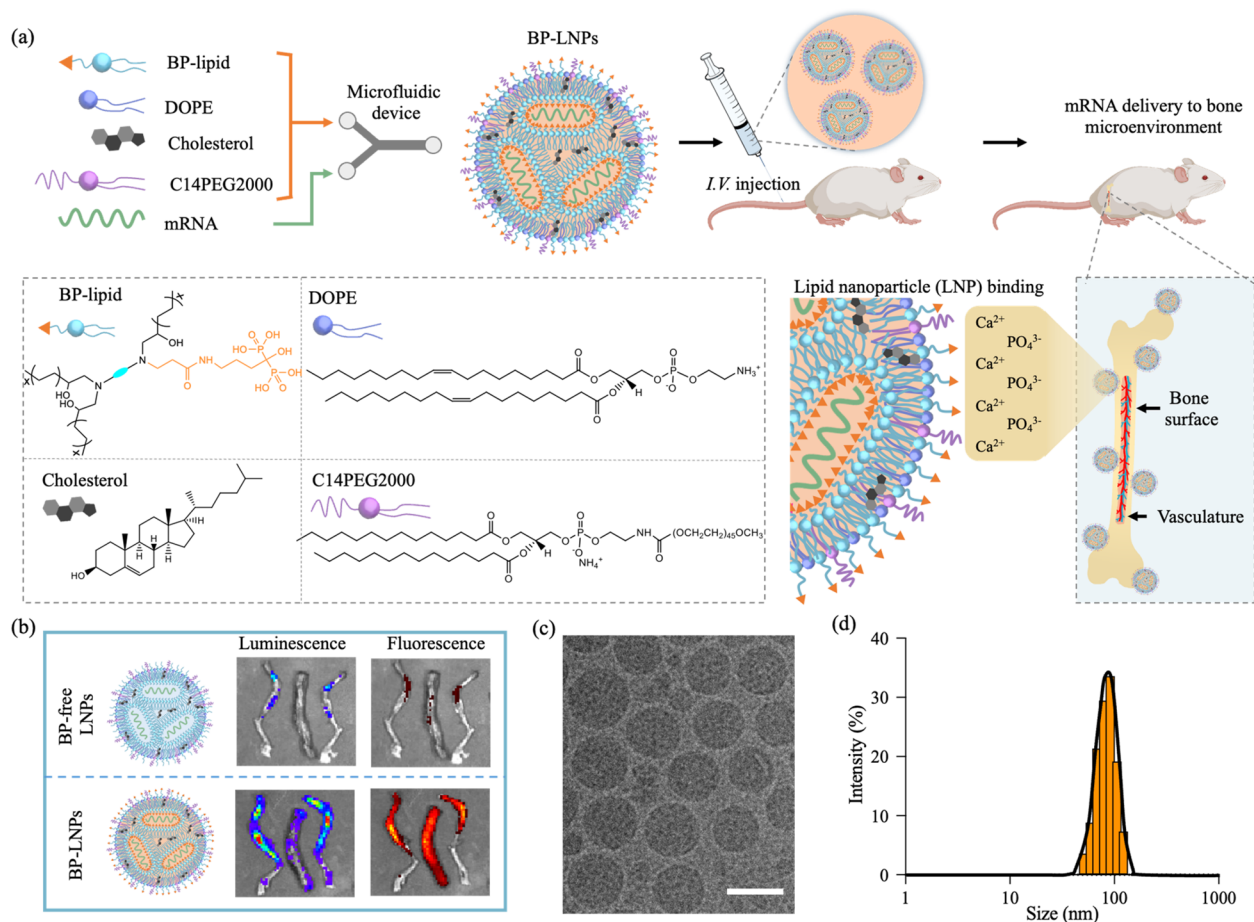


**Figure 1.** Rational design of BP lipid-like materials for mRNA delivery to the bone microenvironment *in vivo*. (a) Schematic illustration of lipid nanoparticles (LNPs) containing BP lipid-like materials (BP-LNPs) to enable systemic delivery of mRNA to the bone microenvironment. LNPs were prepared by combining four components (BP-lipid, DOPE, cholesterol, and C14PEG2000) into each formulation using a microfluidic mixing device. After systemic delivery via intravenous injection, BP-LNPs coordinated with calcium ions ( $\text{Ca}^{2+}$ ) in the bone microenvironment to enable specific bone targeting. (b) *Ex vivo* luminescence and fluorescence imaging of bones (left to right: left leg, spine, and right leg) after delivery of LNPs encapsulating luciferase-encoding mRNA, where LNPs are labeled with 1,1'-dioctadecyl-3,3,3',3'-tetramethylindotricarbocyanine iodide (DiR) at a concentration of  $10 \mu\text{g}/\text{mL}$ . A luminescent signal is generated where luciferase mRNA is translated, and fluorescence indicates LNP biodistribution by the DiR signal. (c) Representative cryogenic transmission electron microscopy (cryo-TEM) image showing the morphology of BP-LNPs. Scale bar: 100 nm. (d) Hydrodynamic size distribution of a representative BP-LNP. I.V. = intravenous.

most clinically advanced nonviral delivery vectors for RNA therapeutics are lipid nanoparticles (LNPs), a four-component formulation consisting of ionizable lipids, cholesterol, phospholipids, and poly(ethylene glycol) (PEG)-conjugated lipids, which are used in Alnylam Pharmaceutical's siRNA therapeutic ONPATRO and the COVID-19 mRNA vaccines produced by Pfizer/BioNTech and Moderna, respectively.<sup>33–37</sup> These nanocarriers are biocompatible, can be reproducibly manufactured to encapsulate a range of nucleic acids, and have physical characteristics suitable for various administration routes. Recently, LNPs encapsulating siRNA were systemically delivered to bone marrow cells to silence genes in inflammatory monocytes and endothelial cells to selectively inhibit migration of these cells and their progeny.<sup>38,39</sup> Despite this encouraging progress, passive diffusion of LNPs still makes them extremely challenging to specifically deliver mRNA to the bone microenvironment. Thus, there is a critical unmet need to develop a targeted LNP technology for mRNA delivery to bone. Previous studies have demonstrated that ligand substitution is a promising approach for targeted mRNA LNP therapeutic delivery;<sup>40–42</sup> for instance, Peer and co-

workers demonstrated that primary lymphocytes could be robustly silenced by attaching a pan leukocyte selective targeting ligand onto LNP formulations.<sup>41</sup> Therefore, similar approaches incorporating ligands with affinity for bone could enhance LNP targeting and accumulation in the bone microenvironment. Among various targeting ligands,<sup>43,44</sup> bisphosphonates (BP), such as alendronate, are analogues of inorganic pyrophosphate and can chelate strongly with the calcium ion ( $\text{Ca}^{2+}$ ) of hydroxyapatite (HA), which is the main inorganic component of bone, endowing bisphosphonates with strong affinity and rapid adsorption to the bone surface.<sup>45–48</sup> After administration of BP-LNPs, strong interactions between the bone-targeting ligand on the LNP surface and HA could improve retention and accumulation of LNPs in the bone microenvironment.

Herein, we report the rational design and synthesis of a series of BP-conjugated ionizable lipid-like materials and formulate a library of BP-LNPs for systemic delivery of mRNA to the bone microenvironment (Figure 1a,b). A library of 21 BP-functionalized ionizable lipids were investigated to formulate a library of BP-LNPs with a narrow size distribution

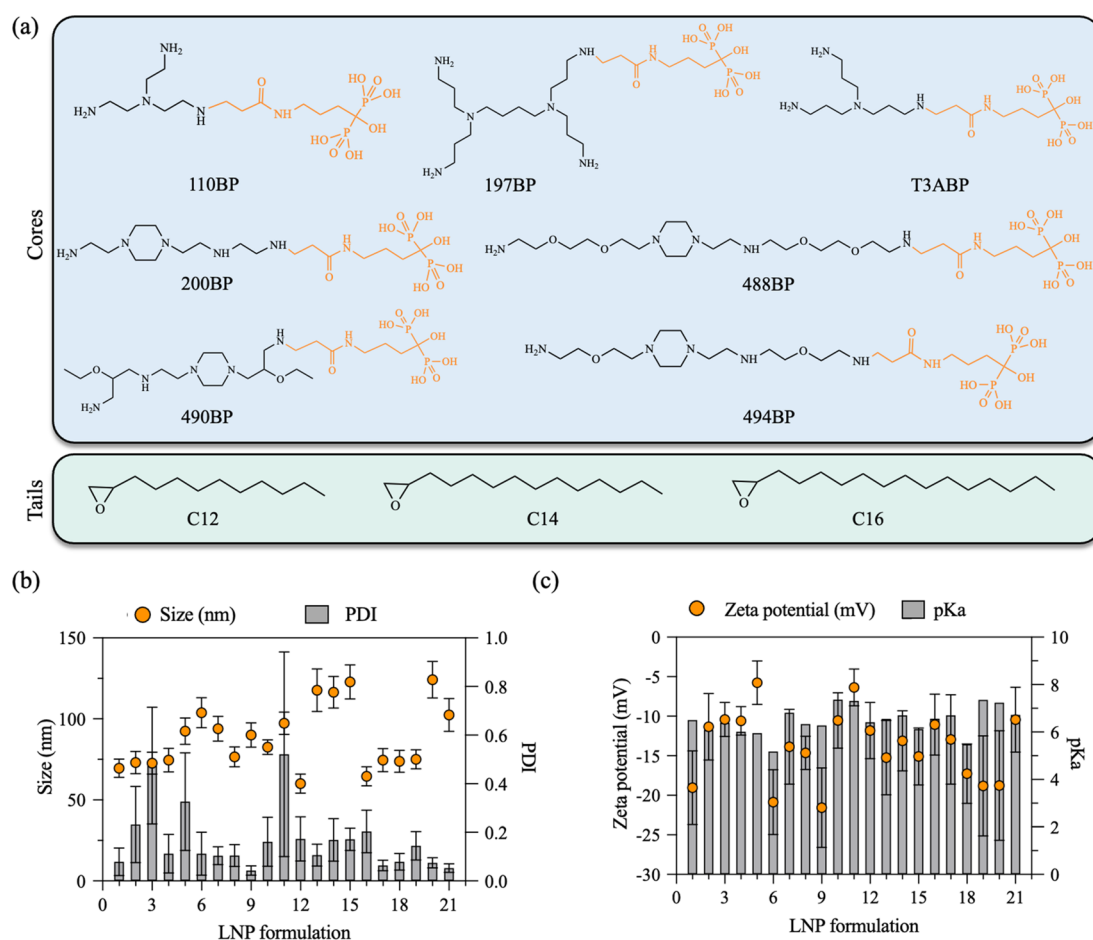


**Figure 2.** A combinatorial library of BP lipid-like materials for mRNA delivery. (a) Chemical structures of 7 alendronate-conjugated polyamine cores (top) and 3 epoxide-terminated alkyl tails (bottom) for generating 21 BP lipids used in this study. BP-LNPs are named based on their BP-conjugated ionizable lipid component consisting of a BP-functionalized polyamine core (110BP, 197BP, T3ABP, 200BP, 488BP, 490BP, and 494BP) and alkyl tail of varying chain lengths (C12, C14, and C16). (b) Hydrodynamic size and polydispersity index (PDI) of the 21 formulated BP-LNPs. (c) Characterization of zeta potential and  $pK_a$  for each BP-LNP formulation. Error bars represent SD.

(Figure 1c,d). Following an initial *in vitro* HeLa cell screening with firefly luciferase-encoding mRNA, 490BP-C14 LNP was identified as the lead formulation, which showed higher protein expression (2.5-fold) compared to LNPs in the absence of BPs (490-C14 LNP). These BP-functionalized LNPs not only displayed higher affinity for both HA and bone surfaces *in vitro* and *ex vivo* but also showed enhanced accumulation and transfection efficiency in the bone microenvironment following systemic administration *in vivo* (Figure 1b). Additionally, 490BP-C14 LNPs exhibited enhanced transfection and uptake in a range of cell types in bone marrow, ranging from B cells, T cells, monocytes, and granulocytes to endothelial cells. Furthermore, BP-LNPs mediated the secretion of bone morphogenetic protein-2 (BMP-2) in the bone microenvironment (both on the bone surface and in the bone marrow) following delivery of BMP-2 mRNA via intravenous injection, demonstrating the therapeutic potential for future applications in bone regeneration and fracture healing. Because of the facile and versatile preparation of BP lipid-like materials, they can potentially be applied toward a range of mRNA LNP bone therapeutic applications including regenerative medicine, protein replacement, and gene editing therapies.

## 2. RESULTS AND DISCUSSION

### 2.1. Rational Design and Synthesis of BP-Functionalized Ionizable Lipids and Incorporation into LNP Formulations.

To enable bone microenvironment targeting of LNP formulations, a series of BP lipid-like materials consisting of alendronate, a type of BP, were designed and synthesized (Figure 2a and Scheme S1). First, alendronate acrylamide was synthesized by reacting alendronate sodium with *N*-acryloxysuccinimide (Scheme S1, Figures S1 and S2). The sodium salt was removed under acidic environments.<sup>49</sup> Then, alendronate acrylamide was conjugated onto amine cores through a Michael addition reaction with a feeding molar ratio of 1:5,<sup>50</sup> yielding alendronate-bearing amine cores. These structures were characterized by <sup>1</sup>H NMR spectra and LC-MS analysis (Figures S2–S9), demonstrating the obtained core structures are not unique as each amine of the cores has the potential to conjugate alendronate, but there should be only one alendronate molecule featured on each core (Figure 2a).

Following synthesis of alendronate-bearing amine cores, a library of 21 BP lipids were synthesized by reacting the alendronate-bearing amine cores with epoxide-terminated alkyl chains (Figure 2a and Figure S10).<sup>51,52</sup> These BP lipids were then mixed with the phospholipid DOPE, cholesterol, lipid-anchored poly(ethylene glycol) (C14PEG2000), and mRNA

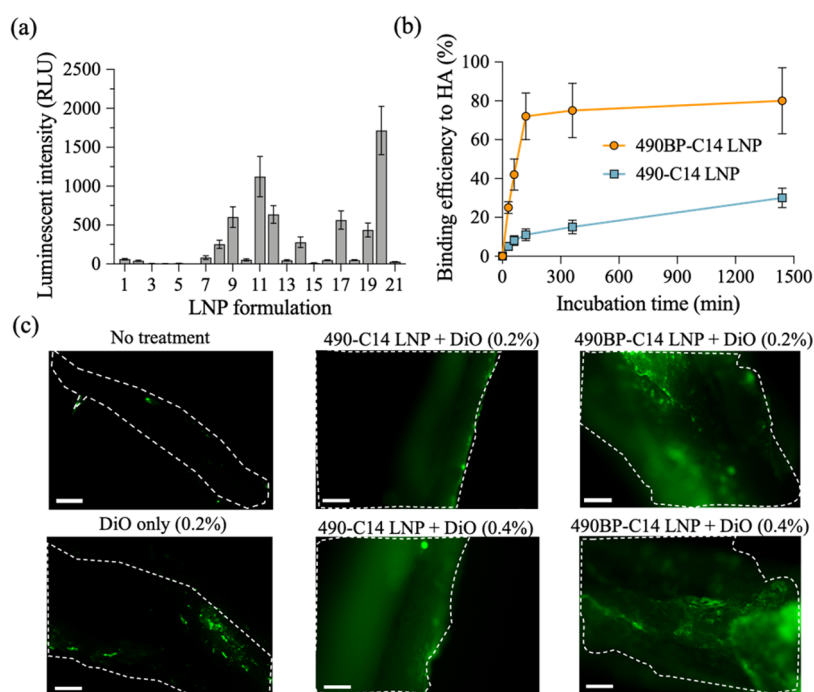


**Figure 3.** *In vitro* screening of BP-LNPs and their binding affinity to HA nanoparticles and bone fragments. (a) Luciferase expression in HeLa cells after treatment with the BP-LNP library encapsulating Fluc mRNA. 5000 cells were incubated with LNPs at a mRNA dose of 10 ng/well. Results were normalized to untreated cells.  $n = 3$  biological replicates. (b) Quantitative evaluation of HA binding kinetics of 490BP-C14 LNPs and 490-C14 LNPs in the absence of BPs (single emulsion). Error bars in (a) and (b) represent SEM. (c) Representative fluorescence images of bone fragments before and after incubation with DiO solution (left), DiO-labeled 490-C14 LNPs (center), and DiO-labeled targeted 490BP-C14 LNPs (right). All samples were washed with PBS before imaging. Bone fragments were acquired from mouse femurs. Scale bar: 200  $\mu\text{m}$ .

via perfusion through a microfluidic mixing device that is designed with herringbone features to induce chaotic mixing.<sup>53–55</sup> The naming of LNP formulations represents both the unique alendronate-conjugated amine core component (labeled as 110BP, 197BP, T3ABP, 200BP, 488BP, 490BP, and 494BP) and the alkyl chain length (C12, C14, and C16) (Figure 2a). In these LNPs, the ionizable lipid enables cellular uptake and endosomal escape to deliver encapsulated mRNA into the cytosol.<sup>56</sup> DOPE and cholesterol enhance LNP stability, improve mRNA encapsulation, and assist in endosomal escape.<sup>57,58</sup> PEG lipid (C14PEG2000) promotes overall LNP stability and prolongs LNP circulation *in vivo*.<sup>59</sup> To demonstrate increased delivery to bone after the introduction of alendronate molecules, another LNP library without BP modification was formulated and used as a control (Figure S11).

The resulting BP-LNPs were characterized to evaluate particle size, polydispersity index (PDI), zeta potential,  $pK_a$ , and mRNA encapsulation efficiency.<sup>55,60</sup> The hydrodynamic diameter for all BP-LNP formulations ranged from 60.1 to 124.2 nm by intensity measurements using dynamic light scattering (DLS) (Figure 2b). Most BP-LNP formulations (>80%) were highly monodisperse, with a PDI value less than 0.2 (Figure 2b). Owing to the incorporation of negatively charged alendronate molecules, BP-LNPs had a negative zeta potential (Figure 2c).<sup>61</sup> The mRNA encapsulation efficiency of BP-LNPs was assessed by a fluorescent RiboGreen assay, where most efficiencies ranged from 60 to 90%, while some LNPs containing BP lipid-like materials with a C16 alkyl chain could not formulate stable mRNA LNPs due to their weak solubility during formulation (Figure S12). Additionally, BP-LNPs were evaluated for their  $pK_a$ , which indicates the pH at

which BP-LNPs are 50% protonated (Figure 2c and Figure S13). In previous studies,  $pK_a$  values between 6 and 7 were commonly reported for successful nucleic acid delivery as LNPs can become protonated in acidic endosomes within this range and can induce fusion with endosomal membranes to release mRNA into the cytosol.<sup>62–64</sup>  $pK_a$  values of BP-LNP formulations ranged from 5.18 to 7.35 (Figure 2c), demonstrating that >70% of the LNPs were within the desired range ( $pK_a$  6.0–7.0) for successful endosomal escape and mRNA delivery. In addition, BP-LNPs exhibited high stability when stored over time. There was no significant size change or decrease in encapsulation efficiency when 490BP-C14 LNPs were stored at 4 °C for 21 days (Figure S14a,b); additionally, BP-LNPs maintained relatively high levels of *in vitro* transfection (Figure S14c).

**2.2. BP-LNP *In Vitro* Screening, *In Vitro* Binding with Hydroxyapatite, and *Ex Vivo* Affinity to Bone.** To evaluate BP-LNPs for their ability to deliver mRNA, mRNA encoding for luciferase was chosen as a reporter gene. Firefly luciferase (FLuc) mRNA with N1-Methyl-PseudoU modifications was used for screening *in vitro* and *in vivo*.<sup>65,66</sup> These modifications have been shown to improve mRNA encapsulation efficiency, reduce overall immunogenicity, and enhance the potency of mRNA.<sup>65,67,68</sup> Here, BP-LNP-mediated delivery of FLuc mRNA was assessed in HeLa cells, a cell line utilized for rapid *in vitro* screening of LNP formulations, for FLuc expression and cell viability. After treatment with BP-LNPs for 24 h at a concentration of 10 ng/5000 cells, luciferase expression was evaluated via luminescence measurements, which were normalized to an untreated control group. These results allowed for determination of structure–activity relationships (SARs) with respect to epoxide-terminated alkyl tails and

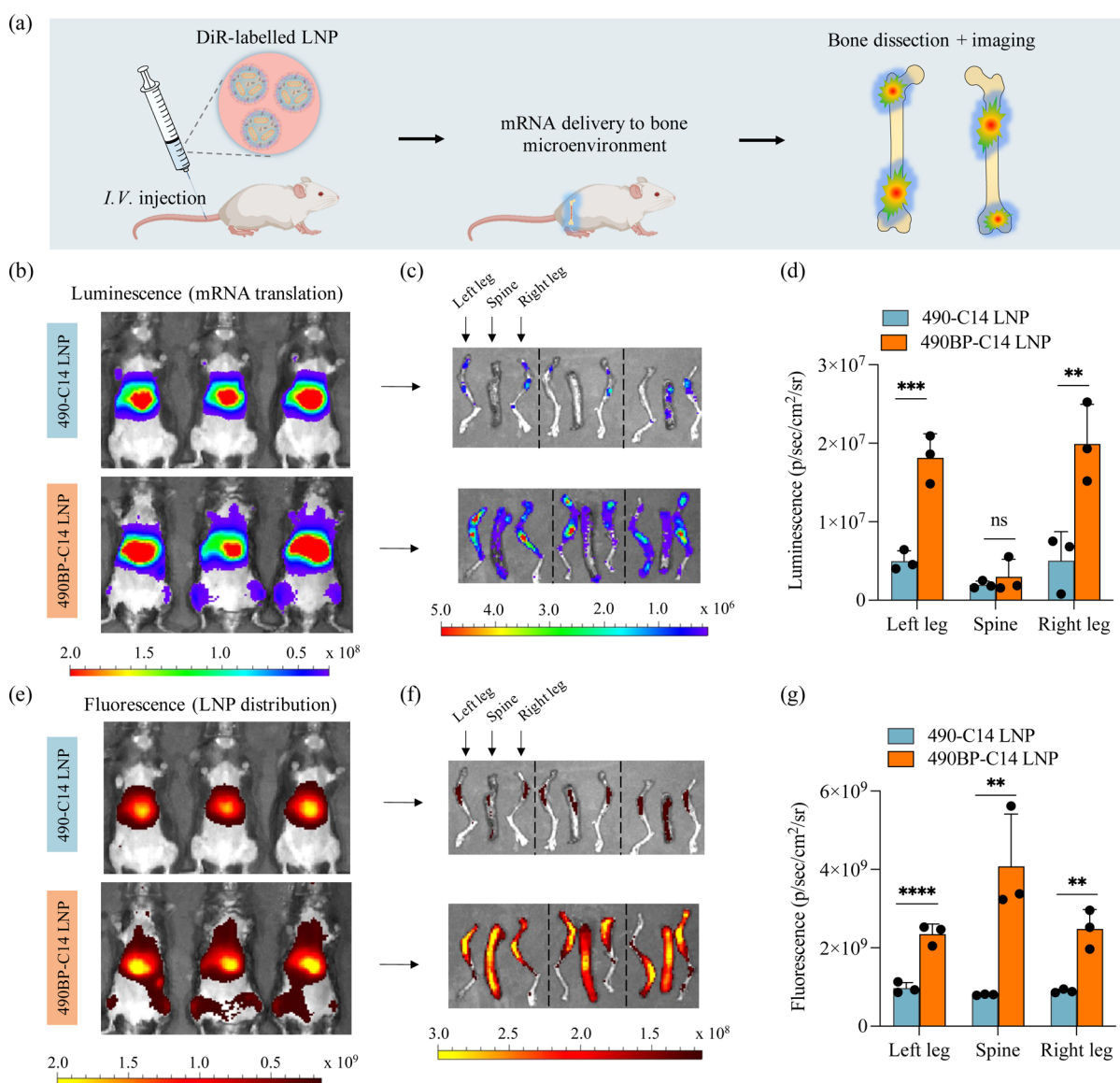


**Figure 4.** *In vivo* mRNA delivery and biodistribution of BP-LNPs to the bone microenvironment. (a) Schematic illustration of DiR-labeled LNPs delivering mRNA to the bone of mice. Bone fragments were further dissected for quantifying the transfection and homing efficiency of BP-LNPs. (b) IVIS imaging of FLuc mRNA delivery to mice by 490-C14 and 490BP-C14 LNPs. Bone fragments show high luminescence intensity after 490BP-C14 LNP treatment.  $n = 3$  mice. (c) Left leg, spine, and right leg were dissected for luminescence imaging. (d) Total luminescence quantification of the dissected left leg, spine, and right leg for 490-C14 LNP- and 490BP-C14 LNP-treated mice. (e) *In vivo* biodistribution of DiR-labeled LNPs, where the whole skeleton showed increased fluorescence signal following treatment by BP-LNPs.  $n = 3$  mice. (f) Left leg, spine, and right leg were dissected for fluorescence imaging. (g) Total fluorescence of the dissected left leg, spine, and right leg for 490-C14 LNP- and 490BP-C14 LNP-treated mice. Statistical significance in (d) and (g) was calculated by using a Student's *t* test with unpaired design. \*\*\*\* $P < 0.0001$ ; \*\*\* $P < 0.001$ ; \*\* $P < 0.01$ . Error bars represent SEM.

alendronate-amine core chemical structures, where five BP-LNPs resulted in similar or even higher luciferase expression compared to a standard LNP formulation by using C12-200 as the ionizable lipid (Figure 3a and Figure S15).<sup>69</sup> All LNP formulations demonstrated low cytotoxicity; three formulations resulted in cell viabilities between 70% and 80%, while the remaining LNP formulations resulted in cell viabilities >80% (Figure S16). To further evaluate how BP affects the ability of LNPs to deliver mRNA, a series of LNPs that did not incorporate BPs were formulated as controls (Figures S11 and S15). Among all of the LNP formulations examined in the initial screening, 490BP-C14 LNP was identified as the top formulation, as it demonstrated 2.5 times higher transfection

compared to 490-C14 LNPs in the absence of BPs (Figure S17a). 490BP-C14 LNPs also demonstrated mRNA dose-dependent transfection of HeLa cells, showing increased luminescence intensity with increasing FLuc mRNA dosage (Figure S17b). Therefore, we selected 490BP-C14 as the lead LNP formulation to further evaluate its ability to target bone for enhanced delivery of mRNA *in vitro* and *in vivo*.

To visualize the bone-binding efficiency of these BP-LNPs, a DiO fluorescence molecule was incorporated into both BP-LNPs and LNPs without BPs.<sup>70</sup> As the bone microenvironment is rich in HA, we first performed an HA binding assay with 490BP-LNPs compared to 490-C14 LNPs that do not contain BPs (Figure 3b). After incubation with HA nano-

particles, 490BP-C14 LNPs showed fast and efficient binding to HA (Figure 3b) because of the strong chelation of BPs on the LNP surface with HA.<sup>26,71</sup> After a 2 h incubation, HA binding of BP-LNPs increased to 80%, significantly higher than LNPs without BPs (10%). After this time course, the binding efficiency plateaued with increased incubation time. The affinity of BP-LNPs to HA in bone fragments was further confirmed by fluorescence microscopy (Figure 3c). Minimal fluorescence was detected on DiO-treated bone samples, indicating low binding between free DiO molecules and the bone surface. After treatment with DiO-labeled 490-C14 LNPs, a very weak fluorescence signal was generated, which may result from passive accumulation of LNPs on the bone surface. This weak fluorescence signal could be improved by increasing the DiO concentration in 490-C14 LNPs. However, 490BP-C14 LNPs exhibited the strongest binding affinity to bone fragments, implying that the incorporation of BPs enables LNP targeting to bone. These results demonstrate the impact of the design of our targeted BP-LNPs in bone mineral binding and the differential binding of targeted BP-LNPs that facilitated the following *in vivo* studies.

**2.3. *In Vivo* Transfection and Biodistribution Studies of BP-LNPs.** Following confirmation of the *in vitro* and *ex vivo* bone-targeting ability of BP-conjugated LNPs, *in vivo* transfection and biodistribution studies were used to investigate the bone-homing ability of BP-LNPs by using C57BL/6J mice following intravenous injection of 0.5 mg/kg FLuc mRNA. Fluorescent DiR was used to track LNP biodistribution by using an *in vivo* imaging system (IVIS) (Figure 4a). After 12 h, functional delivery of FLuc mRNA was observed in the liver and bones (Figure 4b–d and Figure S18). The luminescent intensity of the hind limbs was significantly higher following delivery of BP-LNPs (Figure 4b). Bones from the hind limbs, spines (Figure 4c), and fore limbs (Figure S19) of mice were dissected to evaluate luminescent intensity by quantifying radiance efficiency, where LNPs without BPs showed very low transfection in the dissected bones. While BP-LNPs transfected cells on bone surfaces weakly in the fore limbs and spine, they exhibited strong transfection in the hind limbs such as the femur and tibia (Figure 4d). The mean transfection efficiency of the left leg, spine, and right leg increased 3.7-, 1.8-, and 3.7-fold, respectively, with BP-LNPs compared to LNPs without BPs. The biodistribution of BP-LNPs was then investigated (Figure 4e–g). While LNPs without BPs mainly accumulated in the liver, BP-LNP biodistribution was more widespread in the liver, spleen and bone-dense regions (Figure 4e). By observation of the biodistribution of BP-LNPs over time, the fluorescence intensity of the whole body of mice increased, implying the adsorption of BP-LNPs during circulation (Figure S20).<sup>71</sup> For further examination of bone targeting, dissected legs and spine were evaluated by quantifying the fluorescent intensity (Figure 4f). All BP-LNP-treated bone samples exhibited significantly increased fluorescence (Figure 4g), with approximately 2.5-, 4.5-, and 2.4-fold increase in the left leg, spine, and right leg, respectively, compared to LNPs without BPs. Although we observed significantly higher 490BP-C14 LNP accumulation in the spine, we observed no detrimental off-target effects based on hematoxylin and eosin (H&E) staining (Figure S21). Thus, *in vivo* transfection and biodistribution studies complement the *in vitro* and *ex vivo* high bone binding efficiency of BP-LNPs, highlighting their potential for bone-targeted mRNA delivery.

**2.4. *In Vivo* BP-LNP Transfection and Distribution of Diverse Cell Types in Bone and Bone Marrow.** Having established that 490BP-C14 LNPs can increase mRNA delivery to the bone microenvironment, we then performed immunostaining analysis to evaluate delivery to anatomical regions in the bone microenvironment. To demonstrate this, 490BP-C14 LNP formulated with mRNA encoding for enhanced green fluorescent protein (EGFP) was administered into mice. We then performed paraffin section analysis to assess EGFP transfection in the metaphysis, central marrow, and endosteum of femurs (Figure 5). We demonstrated that (1) the EGFP

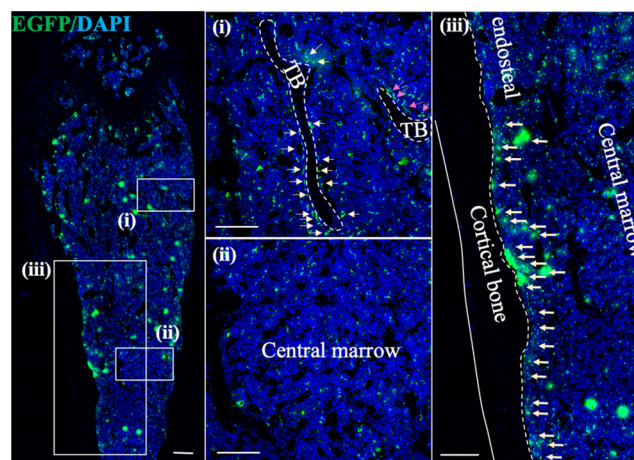


**Figure 5.** Representative images of EGFP expression in the femur after administration of 490BP-C14 LNPs encapsulating EGFP mRNA to the bone microenvironment by intravenous injection. The bone femur was dissected 12 h post injection. DAPI was used for nuclear staining. The mRNA dosage was 0.5 mg/kg. EGFP expression was detected in the bone marrow, especially in the endosteum, rather than on the bone surface.

signal was detected in metaphyseal bone marrow near the trabecular bone surface [magnification of bone part (i), Figure 5], (2) the EGFP signal was widely distributed in the central marrow [magnification of bone part (ii), Figure 5], and (3) EGFP transfection was observed in endosteal bone marrow near the bone surface [magnification of bone part (iii), Figure 5]. These observations indicate that cells in the bone marrow, especially endosteal cells, can be transfected, rather than the cells on the bone surface.

Because bone marrow is the primary hematopoietic organ and a residence site of diverse cell types,<sup>1,6,10</sup> we then evaluated the targeting of specific cell types in bone marrow. To demonstrate this, EGFP-encoding mRNA was administered into mice, and flow cytometry was performed on cells isolated from bone marrow to identify transfection of different cell types. Specifically, DiR-labeled 490BP-C14 LNPs encapsulating EGFP mRNA were formulated and administered intravenously at 0.5 mg/kg alongside PBS and 490-C14 LNP control groups. After 12 h, mice were sacrificed, bone marrow was isolated, red blood cells were lysed, and the remaining cells were analyzed using flow cytometry. Flow cytometry analysis was conducted on diverse cell populations: monocytic lineage (CD11b<sup>+</sup>), B cell lineage (CD45R/B220<sup>+</sup>), T cells (CD3<sup>+</sup>), monocytes (Ly6c<sup>+</sup>), endothelial cells (CD31<sup>+</sup>), granulocytes (Ly6G<sup>+</sup>), B cells (CD19<sup>+</sup>), and hematopoietic stem cells (HSCs, stem cell antigen-1, SCA-1<sup>+</sup>) (Figure 6 and Figure S22). Compared to the 490-C14 LNP treatment group, EGFP

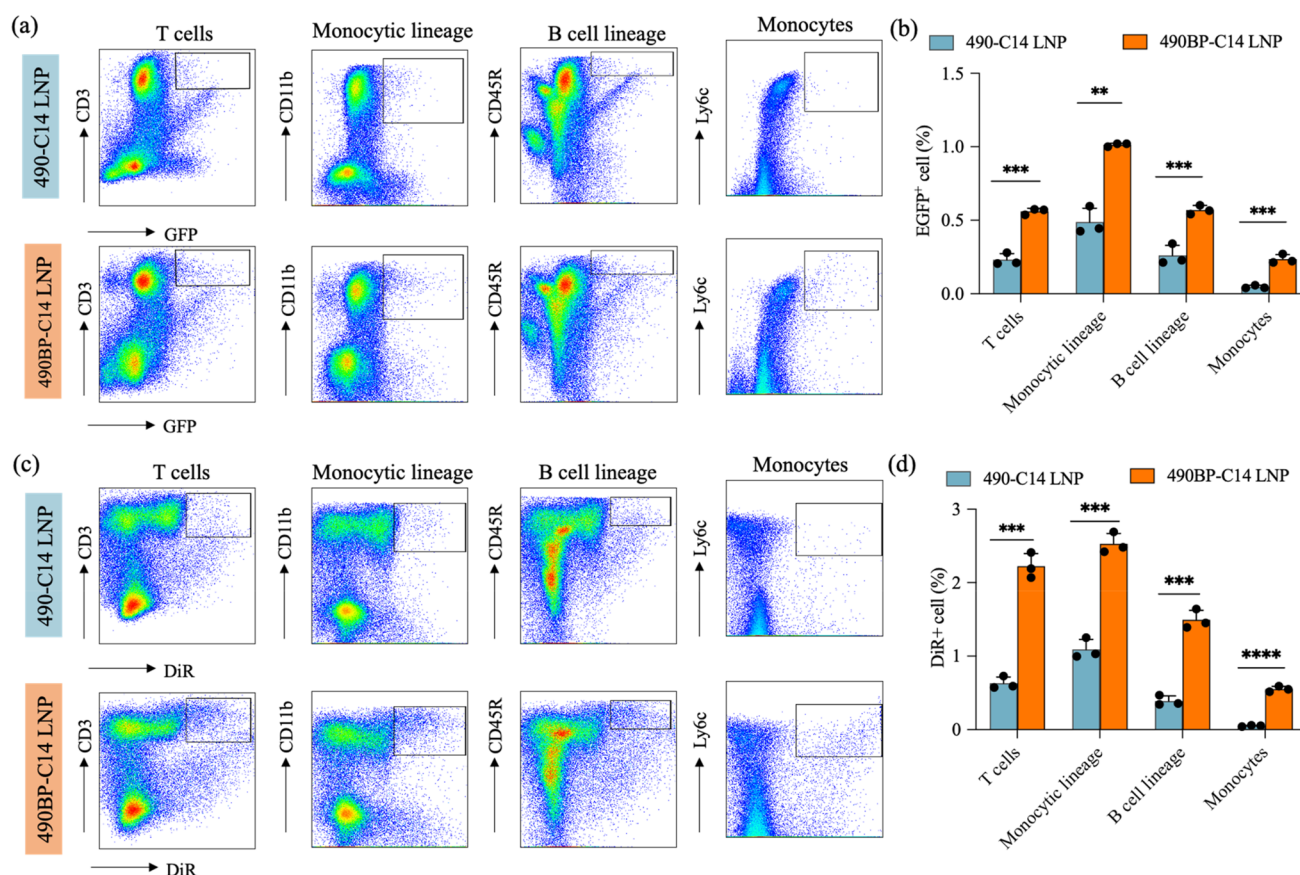


**Figure 6.** Bone and bone marrow cell transfection and distribution following mRNA delivery using BP-LNPs. (a) Gating for EGFP mRNA transfection in different cell types by 490-C14 and 490BP-C14 LNPs. T cells, monocytic lineage, B cell lineage, and monocytes were labeled by their corresponding markers. (b) Different EGFP<sup>+</sup> cell populations following treatment with LNPs that incorporate (490BP-C14) or do not incorporate (490-C14) bone-targeting BPs. (c) Gating for DiR fluorescence in different cell types treated with 490-C14 and 490BP-C14 LNPs. T cells, monocytic lineage, B cell lineage, and monocytes were labeled by their corresponding markers. (d) Different DiR<sup>+</sup> cell populations following treatment with DiR-loaded LNPs.  $n = 3$  mice. Statistical significance in (b) and (d) was calculated by using a Student's  $t$  test with unpaired design. \*\*\*\* $p < 0.0001$ ; \*\*\* $p < 0.001$ ; \*\* $p < 0.01$ . Error bars represent SEM.

transfection efficiency was enhanced in T cells, monocytic lineage cells, and B lineage cells as well as a small increase in B cells, endothelial cells, granulocytes, and HSCs following delivery of BP-LNPs (Figure 6a,b and Figure S22). Interestingly, 490BP-C14 LNPs exhibited over 4-fold higher transfection efficiency to monocytes than 490-C14 LNPs (Figure S23).<sup>38,39</sup> Similarly, 490BP-C14 LNPs exhibited slightly higher EGFP transfection in HSCs than 490-C14 LNPs.<sup>72</sup> In addition to quantification of mRNA functional delivery, LNP biodistribution to bone marrow cells was investigated. BP-LNPs had increased accumulation in diverse cell types, such as T cells, monocytic lineage cells, B lineage cells, and monocytes compared to LNPs without BPs (Figure 6c,d). This increased accumulation was in agreement with the results from EGFP transfection efficiency (Figure S23), where BP-LNP accumulation in monocytes increased over 10-fold compared with LNPs without BPs. Differing from the populations of EGFP<sup>+</sup> cells, endothelial cells exhibited the highest BP-LNP uptake ability, likely because a portion of BP-LNPs could not pass through the blood–bone barrier after intravenous administration (Figure S22).<sup>73</sup>

**2.5. BMP-2 Secretion after Delivery of BMP-2 mRNA to the Bone Microenvironment Using BP-LNPs.** Having established BP-LNPs for enhanced systemic delivery of mRNA to the bone microenvironment, we then evaluated the delivery

potential of mRNA encoding functional BMP-2. BMP-2 is a multifunctional growth factor belonging to the transforming growth factor-beta (TGF- $\beta$ ) superfamily, which plays an important role in the process of bone induction that stimulates osteogenic differentiation.<sup>74,75</sup> Therefore, increased expression of BMP-2 in the bone microenvironment may lead to new opportunities for a variety of therapeutic interventions, such as bone defects, nonunion fractures, osteoporosis treatment, and root canal therapy.<sup>1,46</sup> After BP-LNPs incorporating mRNA encoding for BMP-2 were delivered by intravenous injection, BMP-2 levels on the bone surface and in the bone marrow were quantified (Figure 7a). It was noted that BMP-2 is normally secreted in the bone microenvironment, and thus we also observed BMP-2 secretion both on the bone surface (Figure 7b) and in the bone marrow (Figure 7c) from the PBS-treated control group. Although LNPs without BPs could increase BMP-2 secretion in the bone microenvironment to some extent, BP-LNPs significantly increased BMP-2 expression (Figure 7b,c). Furthermore, BMP-2 levels in the bone microenvironment increased with increasing BMP-2 mRNA dosage (Figure 7b,c), which were as high as 2.3 and 5.3 pg/mg on the bone surface and in the bone marrow, respectively, at a mRNA dosage of 1.5 mg/kg, demonstrating potential for bone regeneration and fracture healing.

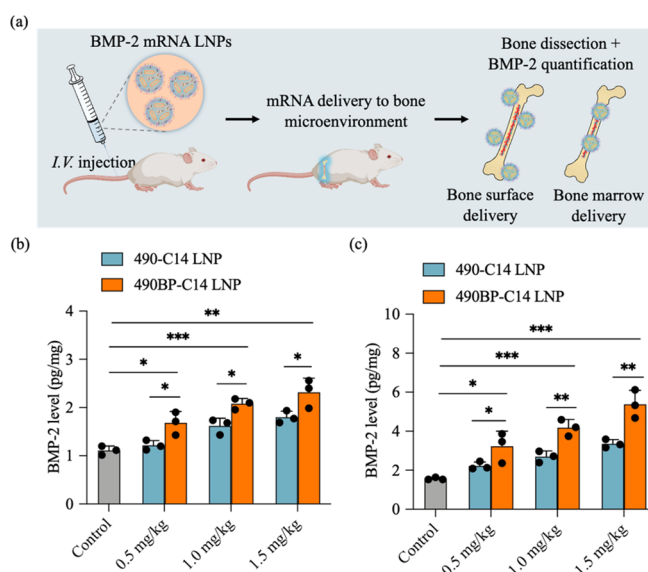


**Figure 7.** BMP-2 protein secretion in the bone microenvironment following delivery of BP-LNPs encapsulating mRNA encoding for BMP-2 via intravenous injection. (a) Schematic illustration of LNPs delivering BMP-2 mRNA to the bone of mice. Bone fragments were dissected to quantify the secretion of BMP-2 on the bone surface and in the bone marrow. (b) BMP-2 secretion from the bone surface following BP-LNP mRNA delivery. BMP-2 was extracted from the bone surface by incubating bone samples with 4 M guanidine hydrochloride overnight. (c) BMP-2 secretion in bone marrow with increased BMP-2 mRNA dosing. BMP-2 was extracted from bone marrow.  $n = 3$  mice. Statistical significance in (b) and (c) was calculated using a Student's  $t$  test with unpaired design. \*\*\*  $P < 0.001$ ; \*\*  $P < 0.01$ ; \*  $P < 0.05$ . Error bars represent SEM.

To further characterize BMP-2 expression, whole tibia bones from mice were then dissected for immunofluorescence (IF) analysis. Compared to low BMP-2 expression in mice treated by PBS (Figure 8a), 490-C14 LNP delivering BMP-2 mRNA demonstrated relatively higher BMP-2 expression on both the trabecular and cortical bone surfaces (Figure 8b). In addition, 490BP-C14 LNPs delivering BMP-2 mRNA demonstrated significantly higher BMP-2 expression in the metaphyseal and endosteal marrow (Figure 8c). Representative BMP-2 expression regions, such as the growth plate, primary spongiosa, metaphyseal bone marrow (Figure 8, parts a1, b1, and c1), and endosteal region (Figure 8, parts a2, b2, and c2) of the medial anterior tibia were chosen to show the targeted delivery and expression of BMP-2. As shown in the magnified regions (Figure 8), the increase in BMP-2 expression in the metaphyseal and endosteal bone marrow for the 490BP-C14 LNP group illustrates the importance of BP lipid-like materials for mRNA delivery to bone and a potential disease treatment strategy based on BMP-2 expression. However, it is still difficult to characterize the cell populations which express BMP-2 because of (1) the diverse and complex cell populations in bone marrow and (2) the secretion of BMP-2 protein that may influence their internal distribution. To investigate whether proper signaling pathways are activated after BMP-2 mRNA delivery, we performed IF staining of Smad1/5 which is phosphorylated during BMP-2 expression. A noticeable increase in phosphorylated Smad1/5 was detected in cells on the trabecular bone surface (Figure S24a), on the cortical bone surface (Figure S24b), and in bone marrow (Figure S24a,b) after 490BP-C14 LNP delivery of BMP-2

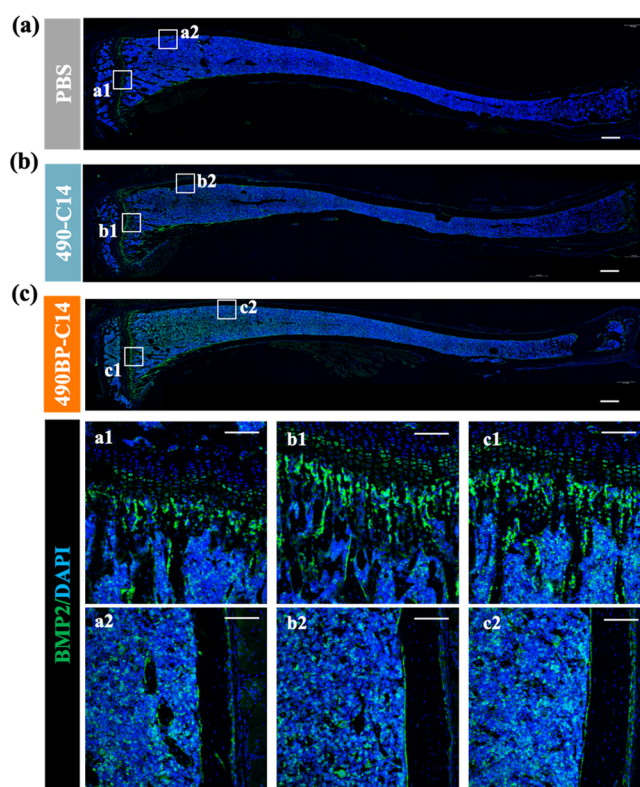


**Figure 8.** Representative immunofluorescence images of BMP-2 expression in the tibia bones of mice. (a) Tibia bone from PBS-treated mice. (b) Tibia bone was dissected from mice treated with 490-C14 LNPs delivering BMP-2 mRNA. (c) Tibia bone was dissected from mice treated with 490BP-C14 LNPs delivering BMP-2 mRNA. The magnified regions represent BMP-2 expression. Scale bar: 500  $\mu\text{m}$ . DAPI (blue) was used for nuclear staining, and BMP-2 expression is shown in green.

mRNA, indicating efficient BMP-2 mRNA delivery to the bone microenvironment and subsequent signaling pathway activation.

Additionally, normal liver function (assessed by aspartate aminotransferase [AST] and alanine aminotransferase [ALT] activities) was shown in mice treated with BP-LNPs, demonstrating that BP-LNPs did not cause notable toxicity *in vivo* (Figure S25). To further evaluate the safety of BP-LNPs, H&E staining was conducted and indicated no toxicity to bone femurs (Figure S26).

Biphosphonate (BP) and BP derivatives have been used as targeting ligands for bone microenvironment-targeted delivery of therapeutic cargoes such as HER-2 targeting Trastuzumab antibody, BMP-2 growth factor, calcium phosphate-DNA plasmid, and parathyroid hormone for disease treatments.<sup>76–79</sup> Unlike traditional gene delivery of DNA, which needs first to translocate to the nucleus of the cell before expression, mRNA can almost immediately be translated into its cognate proteins after delivery to cells without any risk of insertional mutagenesis or genetic damage. Very recently, De La Vega and co-workers used chemically modified mRNA encoding BMP-2 for efficient healing of large osseous segmental defects, providing an innovative and potentially translatable technology for bone healing application.<sup>80</sup> Although these studies made drastic improvements for bone targeting applications, efficient and specific delivery of mRNA to the bone microenvironment still remains a challenge. Thus, we report these BP lipid-like

materials, which incorporate bone-targeting moieties (bisphosphonates) with the most clinically advanced nonviral delivery vectors (LNPs) for therapeutic mRNA delivery. At this site, bisphosphonate could enhance the affinity of the delivery vector to the bone microenvironment, and LNPs could enable mRNA delivery to specific cell types. Our platform demonstrates significant potential for mRNA delivery to diverse cell types in the bone microenvironment with high efficacy and low toxicity. The high accumulation of BP lipid-like materials on bone and the resulting effective secretion of BMP-2 protein in the bone microenvironment provide great potential of mRNA-LNPs therapeutics for bone defect healing.

### 3. CONCLUSIONS

In summary, we developed a facile and versatile approach to engineer a library of BP lipid-like materials that can be formulated into LNPs (BP-LNPs) for systemic delivery of mRNA to the bone microenvironment. The bone-targeting BP ligand alendronate can be easily conjugated onto amine cores to construct a series of novel BP lipid-like materials, which can then form stable bone-homing LNPs when combined with DOPE, cholesterol, and C14-PEG2000 through microfluidic mixing. After an initial assessment from *in vitro* screening, 490BP-C14 LNP was identified as the lead formulation in this library. Compared to LNPs that did not incorporate BP-lipids, 490BP-C14 LNPs showed increased higher hydroxyapatite binding *in vitro* and affinity for bone fragments *ex vivo*. Following systemic delivery, LNP homing and mRNA transfection in the bone microenvironment significantly increased with LNPs incorporating BP lipid-like materials. In addition, 490BP-C14 LNPs showed increased transfection efficiency in diverse cell types in the bone marrow, especially monocytes (4-fold increase compared to LNP without BPs). BMP-2 secretion on the bone surface and in the bone marrow significantly increased after systemic BMP-2 mRNA delivery by 490BP-C14 LNPs. The incorporation of BP lipid-like materials into LNPs demonstrates their potential in targeted mRNA delivery to bone, which can have applications in regenerative medicine, protein replacement, and gene editing therapies for bone and bone marrow. We envision that this generalizable approach to engineer targeted LNPs for enhanced site-specific targeting described here can be expanded to a wealth of additional lipid-like materials in the future to open new avenues for targeted mRNA therapeutics.

### ■ ASSOCIATED CONTENT

#### SI Supporting Information

The Supporting Information is available free of charge at <https://pubs.acs.org/doi/10.1021/jacs.2c02706>.

Materials and instruments; details of synthetic procedures; formulation of BP lipid-like materials into lipid nanoparticles; *in vitro* luciferase mRNA delivery library screening; BP-LNPs stability; *in vitro* bone targeting of LNPs via hydroxyapatite binding; *ex vivo* bone affinity of LNPs; *in vivo* luciferase mRNA LNP delivery; flow cytometry of EGFP mRNA transfected diverse cell types in bone marrow; mRNA-LNP mediated BMP-2 secretion in bone marrow; *in vivo* LNP toxicity measurements; H&E staining of bone femurs; immunofluorescence of Smad1/5 activation (PDF)

### ■ AUTHOR INFORMATION

#### Corresponding Author

**Michael J. Mitchell** – Department of Bioengineering, Abramson Cancer Center, Perelman School of Medicine, Institute for Immunology, Perelman School of Medicine, and Institute for Regenerative Medicine, Perelman School of Medicine, University of Pennsylvania, Philadelphia, Pennsylvania 19104, United States; Cardiovascular Institute, Perelman School of Medicine, University of Pennsylvania, Philadelphia, Pennsylvania 19014, United States; [orcid.org/0000-0002-3628-2244](https://orcid.org/0000-0002-3628-2244); Email: [mjmitch@seas.upenn.edu](mailto:mjmitch@seas.upenn.edu)

#### Authors

- Lulu Xue** – Department of Bioengineering, University of Pennsylvania, Philadelphia, Pennsylvania 19104, United States; [orcid.org/0000-0001-5719-1336](https://orcid.org/0000-0001-5719-1336)
- Ningqiang Gong** – Department of Bioengineering, University of Pennsylvania, Philadelphia, Pennsylvania 19104, United States
- Sarah J. Shepherd** – Department of Bioengineering, University of Pennsylvania, Philadelphia, Pennsylvania 19104, United States
- Xinhong Xiong** – Yangtze Delta Region Institute (Huzhou), University of Electronic Science and Technology of China, Huzhou, Zhejiang 313001, China
- Xueyang Liao** – Translational Research Program of Pediatric Orthopedics, Department of Surgery, The Children's Hospital of Philadelphia, Philadelphia, Pennsylvania 19104, United States
- Xuexiang Han** – Department of Bioengineering, University of Pennsylvania, Philadelphia, Pennsylvania 19104, United States
- Gan Zhao** – Department of Biomedical Sciences, School of Veterinary Medicine, University of Pennsylvania, Philadelphia, Pennsylvania 19104, United States
- Chao Song** – Translational Research Program of Pediatric Orthopedics, Department of Surgery, The Children's Hospital of Philadelphia, Philadelphia, Pennsylvania 19104, United States
- Xisha Huang** – Department of Bioengineering, University of Pennsylvania, Philadelphia, Pennsylvania 19104, United States
- Hanwen Zhang** – Department of Bioengineering, University of Pennsylvania, Philadelphia, Pennsylvania 19104, United States
- Marshall S. Padilla** – Department of Bioengineering, University of Pennsylvania, Philadelphia, Pennsylvania 19104, United States
- Jingya Qin** – Department of Bioengineering, University of Pennsylvania, Philadelphia, Pennsylvania 19104, United States
- Yi Shi** – Department of Materials Science and Engineering, University of Delaware, Newark, Delaware 19716, United States
- Mohamad-Gabriel Alameh** – Department of Medicine, University of Pennsylvania, Philadelphia, Pennsylvania 19104, United States; [orcid.org/0000-0002-5672-6930](https://orcid.org/0000-0002-5672-6930)
- Darrin J. Pochan** – Department of Materials Science and Engineering, University of Delaware, Newark, Delaware 19716, United States; [orcid.org/0000-0002-0454-2339](https://orcid.org/0000-0002-0454-2339)

Karin Wang – Department of Bioengineering, Temple University, Philadelphia, Pennsylvania 19122, United States; [orcid.org/0000-0001-7812-2583](https://orcid.org/0000-0001-7812-2583)

Fanxin Long – Translational Research Program of Pediatric Orthopedics, Department of Surgery, The Children's Hospital of Philadelphia, Philadelphia, Pennsylvania 19104, United States

Drew Weissman – Department of Medicine, University of Pennsylvania, Philadelphia, Pennsylvania 19104, United States; [orcid.org/0000-0002-1501-6510](https://orcid.org/0000-0002-1501-6510)

Complete contact information is available at: <https://pubs.acs.org/10.1021/jacs.2c02706>

## Author Contributions

L.X. and N.G. contributed equally to this work.

## Notes

The authors declare the following competing financial interest(s): L.X. and M.J.M. have filed a patent application based on this work. D.W. is an inventor on several patents related to this work filed by the Trustees of the University of Pennsylvania (11/990,646; 13/585,517; 13/839,023; 13/839,155; 14/456,302; 15/339,363; and 16/299,202).

## ACKNOWLEDGMENTS

M.J.M. acknowledges support from a US National Institutes of Health (NIH) Director's New Innovator Award (DP2 TR002776), a Burroughs Wellcome Fund Career Award at the Scientific Interface (CASI), a US National Science Foundation CAREER Award (CBET-2145491), a grant from the American Cancer Society (129784-IRG-16-188-38-IRG), and the National Institutes of Health (NCI R01 CA241661, NCI R37 CA244911, and NIDDK R01 DK123049). We thank BioRender for providing a platform to create the cartoons and schematics used in the figures.

## ABBREVIATIONS

BP; bisphosphonate; BMP-2; bone morphogenetic protein-2.

## REFERENCES

- (1) Croucher, P. I.; McDonald, M. M.; Martin, T. J. Bone metastasis: the importance of the neighbourhood. *Nat. Rev. Cancer* **2016**, *16* (6), 373–386.
- (2) Hofbauer, L. C.; Bozec, A.; Rauner, M.; Jakob, F.; Perner, S.; Pantel, K. Novel approaches to target the microenvironment of bone metastasis. *Nat. Rev. Clin Oncol* **2021**, *18* (8), 488–505.
- (3) Kawano, Y.; Moschetta, M.; Manier, S.; Glavey, S.; Gorgun, G. T.; Roccaro, A. M.; Anderson, K. C.; Ghobrial, I. M. Targeting the bone marrow microenvironment in multiple myeloma. *Immunol Rev* **2015**, *263* (1), 160–172.
- (4) Onishi, T.; Hayashi, N.; Theriault, R. L.; Hortobagyi, G. N.; Ueno, N. T. Future directions of bone-targeted therapy for metastatic breast cancer. *Nat. Rev. Clin Oncol* **2010**, *7* (11), 641–651.
- (5) Hadjidakis, D. J.; Androulakis, I. I. Bone remodeling. *Ann. N. Y. Acad. Sci.* **2006**, *1092*, 385–396.
- (6) Manolagas, S. C.; Jilka, R. L. Bone marrow, cytokines, and bone remodeling. Emerging insights into the pathophysiology of osteoporosis. *N Engl J. Med.* **1995**, *332* (5), 305–311.
- (7) Kovtonyuk, L. V.; Fritsch, K.; Feng, X.; Manz, M. G.; Takizawa, H. Inflamm-Aging of Hematopoiesis, Hematopoietic Stem Cells, and the Bone Marrow Microenvironment. *Front Immunol* **2016**, *7*, 502–504.
- (8) Sacchetti, B.; Funari, A.; Michienzi, S.; Di Cesare, S.; Piersanti, S.; Saggio, I.; Tagliafico, E.; Ferrari, S.; Robey, P. G.; Riminucci, M.; Bianco, P. Self-renewing osteoprogenitors in bone marrow sinusoids

can organize a hematopoietic microenvironment. *Cell* **2007**, *131* (2), 324–336.

(9) Arron, J. R.; Choi, Y. Bone versus immune system. *Nature* **2000**, *408* (6812), 535–536.

(10) Mercier, F. E.; Ragu, C.; Scadden, D. T. The bone marrow at the crossroads of blood and immunity. *Nat. Rev. Immunol* **2012**, *12* (1), 49–60.

(11) Hess, D.; Li, L.; Martin, M.; Sakano, S.; Hill, D.; Strutt, B.; Thyssen, S.; Gray, D. A.; Bhatia, M. Bone marrow-derived stem cells initiate pancreatic regeneration. *Nat. Biotechnol.* **2003**, *21* (7), 763–770.

(12) Huang, Y. C.; Kaigler, D.; Rice, K. G.; Krebsbach, P. H.; Mooney, D. J. Combined angiogenic and osteogenic factor delivery enhances bone marrow stromal cell-driven bone regeneration. *J. Bone Miner Res.* **2005**, *20* (5), 848–857.

(13) Rodan, G. A.; Martin, T. J. Therapeutic approaches to bone diseases. *Science* **2000**, *289* (5484), 1508–1514.

(14) Yamashita, S.; Katsumi, H.; Hibino, N.; Isobe, Y.; Yagi, Y.; Tanaka, Y.; Yamada, S.; Naito, C.; Yamamoto, A. Development of PEGylated aspartic acid-modified liposome as a bone-targeting carrier for the delivery of paclitaxel and treatment of bone metastasis. *Biomaterials* **2018**, *154*, 74–85.

(15) Lavrador, P.; Gaspar, V. M.; Mano, J. F. Stimuli-responsive nanocarriers for delivery of bone therapeutics - Barriers and progresses. *J. Controlled Release* **2018**, *273*, 51–67.

(16) Soundrapandian, C.; Sa, B.; Datta, S. Organic-inorganic composites for bone drug delivery. *AAPS PharmSciTech* **2009**, *10* (4), 1158–1171.

(17) Kolambkar, Y. M.; Boerckel, J. D.; Dupont, K. M.; Bajin, M.; Huebsch, N.; Mooney, D. J.; Huttmacher, D. W.; Guldberg, R. E. Spatiotemporal delivery of bone morphogenetic protein enhances functional repair of segmental bone defects. *Bone* **2011**, *49* (3), 485–492.

(18) Tozzi, G.; De Mori, A.; Oliveira, A.; Roldo, M. Composite Hydrogels for Bone Regeneration. *Materials* **2016**, *9* (4), 267–290.

(19) Nandi, S. K.; Mukherjee, P.; Roy, S.; Kundu, B.; De, D. K.; Basu, D. Local antibiotic delivery systems for the treatment of osteomyelitis – A review. *Materials Science and Engineering: C* **2009**, *29* (8), 2478–2485.

(20) Hanssen, A. D. Local antibiotic delivery vehicles in the treatment of musculoskeletal infection. *Clin Orthop Relat Res.* **2005**, *437*, 91–96.

(21) Babensee, J. E.; McIntire, L. V.; Mikos, A. G. Growth factor delivery for tissue engineering. *Pharm. Res.* **2000**, *17* (5), 497–504.

(22) De Witte, T. M.; Fratila-Apachitei, L. E.; Zadpoor, A. A.; Peppas, N. A. Bone tissue engineering via growth factor delivery: from scaffolds to complex matrices. *Regen Biomater* **2018**, *5* (4), 197–211.

(23) Vuolteenaho, K.; Moilanen, T.; Moilanen, E. Non-steroidal anti-inflammatory drugs, cyclooxygenase-2 and the bone healing process. *Basic Clin. Pharmacol. Toxicol.* **2008**, *102* (1), 10–14.

(24) Schett, G. Effects of inflammatory and anti-inflammatory cytokines on the bone. *Eur. J. Clin Invest* **2011**, *41* (12), 1361–1366.

(25) Sun, Y. Tumor microenvironment and cancer therapy resistance. *Cancer Lett.* **2016**, *380* (1), 205–215.

(26) Swami, A.; Reagan, M. R.; Basto, P.; Mishima, Y.; Kamaly, N.; Glavey, S.; Zhang, S.; Moschetta, M.; Seevaratnam, D.; Zhang, Y.; Liu, J.; Memarzadeh, M.; Wu, J.; Manier, S.; Shi, J.; Bertrand, N.; Lu, Z. N.; Nagano, K.; Baron, R.; Sacco, A.; Roccaro, A. M.; Farokhzad, O. C.; Ghobrial, I. M. Engineered nanomedicine for myeloma and bone microenvironment targeting. *Proc. Natl. Acad. Sci. U. S. A.* **2014**, *111* (28), 10287–10292.

(27) Mosekilde, L.; Eriksen, E. F.; Charles, P. Effects of Thyroid Hormones on Bone and Mineral Metabolism. *Endocrinology and Metabolism Clinics of North America* **1990**, *19* (1), 35–63.

(28) Kowalski, P. S.; Rudra, A.; Miao, L.; Anderson, D. G. Delivering the Messenger: Advances in Technologies for Therapeutic mRNA Delivery. *Mol. Ther* **2019**, *27* (4), 710–728.

- (29) Chen, Y.; Gao, D. Y.; Huang, L. In vivo delivery of miRNAs for cancer therapy: challenges and strategies. *Adv. Drug Deliv Rev.* **2015**, *81*, 128–141.
- (30) Niidome, T.; Huang, L. Gene therapy progress and prospects: nonviral vectors. *Gene Ther.* **2002**, *9* (24), 1647–1652.
- (31) Sorensen, S. J.; Bailey, M.; Hansen, L. H.; Kroer, N.; Wuertz, S. Studying plasmid horizontal transfer in situ: a critical review. *Nat. Rev. Microbiol.* **2005**, *3* (9), 700–710.
- (32) Hu, B.; Zhong, L.; Weng, Y.; Peng, L.; Huang, Y.; Zhao, Y.; Liang, X. J. Therapeutic siRNA: state of the art. *Signal Transduct Target Ther* **2020**, *5* (1), 101–125.
- (33) Whitehead, K. A.; Langer, R.; Anderson, D. G. Knocking down barriers: advances in siRNA delivery. *Nat. Rev. Drug Discov* **2009**, *8* (2), 129–138.
- (34) Akinc, A.; Maier, M. A.; Manoharan, M.; Fitzgerald, K.; Jayaraman, M.; Barros, S.; Ansell, S.; Du, X.; Hope, M. J.; Madden, T. D.; Mui, B. L.; Semple, S. C.; Tam, Y. K.; Ciufolini, M.; Witzigmann, D.; Kulkarni, J. A.; van der Meel, R.; Cullis, P. R. The Onpatro story and the clinical translation of nanomedicines containing nucleic acid-based drugs. *Nat. Nanotechnol.* **2019**, *14* (12), 1084–1087.
- (35) Hou, X.; Zaks, T.; Langer, R.; Dong, Y. Lipid nanoparticles for mRNA delivery. *Nat. Rev. Mater.* **2021**, *6* (12), 1078–1094.
- (36) Paunovska, K.; Loughrey, D.; Dahlman, J. E. Drug delivery systems for RNA therapeutics. *Nat. Rev. Genet.* **2022**, *23* (5), 265–280.
- (37) Han, X.; Zhang, H.; Butowska, K.; Swingle, K. L.; Alameh, M. G.; Weissman, D.; Mitchell, M. J. An ionizable lipid toolbox for RNA delivery. *Nat. Commun.* **2021**, *12* (1), 7233.
- (38) Leuschner, F.; Dutta, P.; Gorbato, R.; Novobrantseva, T. I.; Donahoe, J. S.; Courties, G.; Lee, K. M.; Kim, J. I.; Markmann, J. F.; Marinelli, B.; Panizzi, P.; Lee, W. W.; Iwamoto, Y.; Milstein, S.; Epstein-Barash, H.; Cantley, W.; Wong, J.; Cortez-Retamozo, V.; Newton, A.; Love, K.; Libby, P.; Pittet, M. J.; Swirski, F. K.; Kotliansky, V.; Langer, R.; Weissleder, R.; Anderson, D. G.; Nahrendorf, M. Therapeutic siRNA silencing in inflammatory monocytes in mice. *Nat. Biotechnol.* **2011**, *29* (11), 1005–1010.
- (39) Krohn-Grimberghe, M.; Mitchell, M. J.; Schloss, M. J.; Khan, O. F.; Courties, G.; Guimaraes, P. P. G.; Rohde, D.; Cremer, S.; Kowalski, P. S.; Sun, Y.; Tan, M.; Webster, J.; Wang, K.; Iwamoto, Y.; Schmidt, S. P.; Wojtkiewicz, G. R.; Nayar, R.; Frodermann, V.; Hulsmans, M.; Chung, A.; Hoyer, F. F.; Swirski, F. K.; Langer, R.; Anderson, D. G.; Nahrendorf, M. Nanoparticle-encapsulated siRNAs for gene silencing in the haematopoietic stem-cell niche. *Nat. Biomed. Eng.* **2020**, *4* (11), 1076–1089.
- (40) Kedmi, R.; Veiga, N.; Ramishetti, S.; Goldsmith, M.; Rosenblum, D.; Dammes, N.; Hazan-Halevy, I.; Nahary, L.; Leviatan-Ben-Arye, S.; Harlev, M.; Behlke, M.; Benhar, I.; Lieberman, J.; Peer, D. A modular platform for targeted RNAi therapeutics. *Nat. Nanotechnol.* **2018**, *13* (3), 214–219.
- (41) Ramishetti, S.; Hazan-Halevy, I.; Palakuri, R.; Chatterjee, S.; Naidu Gonna, S.; Dammes, N.; Freilich, I.; Kolik Shmuel, L.; Danino, D.; Peer, D. A Combinatorial Library of Lipid Nanoparticles for RNA Delivery to Leukocytes. *Adv. Mater.* **2020**, *32* (12), No. e1906128.
- (42) Veiga, N.; Diesendruck, Y.; Peer, D. Targeted lipid nanoparticles for RNA therapeutics and immunomodulation in leukocytes. *Adv. Drug Deliv Rev.* **2020**, *159*, 364–376.
- (43) Liang, C.; Guo, B.; Wu, H.; Shao, N.; Li, D.; Liu, J.; Dang, L.; Wang, C.; Li, H.; Li, S.; Lau, W. K.; Cao, Y.; Yang, Z.; Lu, C.; He, X.; Au, D. W.; Pan, X.; Zhang, B. T.; Lu, C.; Zhang, H.; Yue, K.; Qian, A.; Shang, P.; Xu, J.; Xiao, L.; Bian, Z.; Tan, W.; Liang, Z.; He, F.; Zhang, L.; Lu, A.; Zhang, G. Aptamer-functionalized lipid nanoparticles targeting osteoblasts as a novel RNA interference-based bone anabolic strategy. *Nat. Med.* **2015**, *21* (3), 288–94.
- (44) Gao, X.; Li, L.; Cai, X.; Huang, Q.; Xiao, J.; Cheng, Y. Targeting nanoparticles for diagnosis and therapy of bone tumors: Opportunities and challenges. *Biomaterials* **2021**, *265*, 120404.
- (45) Giger, E. V.; Castagner, B.; Leroux, J. C. Biomedical applications of bisphosphonates. *J. Controlled Release* **2013**, *167* (2), 175–188.
- (46) Farrell, K. B.; Karpeisky, A.; Thamm, D. H.; Zinnen, S. Bisphosphonate conjugation for bone specific drug targeting. *Bone Rep* **2018**, *9*, 47–60.
- (47) Cole, L. E.; Vargo-Gogola, T.; Roeder, R. K. Targeted delivery to bone and mineral deposits using bisphosphonate ligands. *Adv. Drug Deliv Rev.* **2016**, *99*, 12–27.
- (48) Zhou, X.; Cornel, E. J.; He, S.; Du, J. Recent advances in bone-targeting nanoparticles for biomedical applications. *Materials Chemistry Frontiers* **2021**, *5* (18), 6735–6759.
- (49) Lund, B. C.; Abrams, T. E.; Gravely, A. A. Rebuttal to Gravely et al. Validity of PTSD diagnoses in VA administrative data: comparison of VA administrative PTSD diagnoses to self-reported PTSD Checklist scores. *J. Rehabil. Res. Dev.* **2011**, *48* (1), 21–30.
- (50) Miller, J. B.; Zhang, S.; Kos, P.; Xiong, H.; Zhou, K.; Perelman, S. S.; Zhu, H.; Siegwart, D. J. Non-Viral CRISPR/Cas Gene Editing In Vitro and In Vivo Enabled by Synthetic Nanoparticle Co-Delivery of Cas9 mRNA and sgRNA. *Angew. Chem., Int. Ed. Engl.* **2017**, *56* (4), 1059–1063.
- (51) Akinc, A.; Zumbuehl, A.; Goldberg, M.; Leshchiner, E. S.; Busini, V.; Hossain, N.; Bacallado, S. A.; Nguyen, D. N.; Fuller, J.; Alvarez, R.; Borodovsky, A.; Borland, T.; Constien, R.; de Fougerolles, A.; Dorkin, J. R.; Narayanannair Jayaprakash, K.; Jayaraman, M.; John, M.; Kotliansky, V.; Manoharan, M.; Nechev, L.; Qin, J.; Racie, T.; Raitcheva, D.; Rajeev, K. G.; Sah, D. W.; Soutschek, J.; Toudjarska, I.; Vornlocher, H. P.; Zimmermann, T. S.; Langer, R.; Anderson, D. G. A combinatorial library of lipid-like materials for delivery of RNAi therapeutics. *Nat. Biotechnol.* **2008**, *26* (5), 561–569.
- (52) Semple, S. C.; Akinc, A.; Chen, J.; Sandhu, A. P.; Mui, B. L.; Cho, C. K.; Sah, D. W.; Stebbing, D.; Crosley, E. J.; Yaworski, E.; Hafez, I. M.; Dorkin, J. R.; Qin, J.; Lam, K.; Rajeev, K. G.; Wong, K. F.; Jeffs, L. B.; Nechev, L.; Eisenhardt, M. L.; Jayaraman, M.; Kazem, M.; Maier, M. A.; Srinivasulu, M.; Weinstein, M. J.; Chen, Q.; Alvarez, R.; Barros, S. A.; De, S.; Klimuk, S. K.; Borland, T.; Kosovrasti, V.; Cantley, W. L.; Tam, Y. K.; Manoharan, M.; Ciufolini, M. A.; Tracy, M. A.; de Fougerolles, A.; MacLachlan, I.; Cullis, P. R.; Madden, T. D.; Hope, M. J. Rational design of cationic lipids for siRNA delivery. *Nat. Biotechnol.* **2010**, *28* (2), 172–176.
- (53) Chen, D.; Love, K. T.; Chen, Y.; Eltoukhy, A. A.; Kastrop, C.; Sahay, G.; Jeon, A.; Dong, Y.; Whitehead, K. A.; Anderson, D. G. Rapid discovery of potent siRNA-containing lipid nanoparticles enabled by controlled microfluidic formulation. *J. Am. Chem. Soc.* **2012**, *134* (16), 6948–6951.
- (54) Shepherd, S. J.; Warzecha, C. C.; Yadavali, S.; El-Mayta, R.; Alameh, M. G.; Wang, L.; Weissman, D.; Wilson, J. M.; Issadore, D.; Mitchell, M. J. Scalable mRNA and siRNA Lipid Nanoparticle Production Using a Parallelized Microfluidic Device. *Nano Lett.* **2021**, *21* (13), 5671–5680.
- (55) Billingsley, M. M.; Singh, N.; Ravikumara, P.; Zhang, R.; June, C. H.; Mitchell, M. J. Ionizable Lipid Nanoparticle-Mediated mRNA Delivery for Human CAR T Cell Engineering. *Nano Lett.* **2020**, *20* (3), 1578–1589.
- (56) Love, K. T.; Mahon, K. P.; Levins, C. G.; Whitehead, K. A.; Querbes, W.; Dorkin, J. R.; Qin, J.; Cantley, W.; Qin, L. L.; Racie, T.; Frank-Kamenetsky, M.; Yip, K. N.; Alvarez, R.; Sah, D. W.; de Fougerolles, A.; Fitzgerald, K.; Kotliansky, V.; Akinc, A.; Langer, R.; Anderson, D. G. Lipid-like materials for low-dose, in vivo gene silencing. *Proc. Natl. Acad. Sci. U. S. A.* **2010**, *107* (5), 1864–1869.
- (57) Zuhorn, I. S.; Bakowsky, U.; Polushkin, E.; Visser, W. H.; Stuart, M. C.; Engberts, J. B.; Hoekstra, D. Nonbilayer phase of lipoplex-membrane mixture determines endosomal escape of genetic cargo and transfection efficiency. *Mol. Ther.* **2005**, *11* (5), 801–810.
- (58) Allen, T. M.; Cullis, P. R. Liposomal drug delivery systems: from concept to clinical applications. *Adv. Drug Deliv Rev.* **2013**, *65* (1), 36–48.
- (59) Oberli, M. A.; Reichmuth, A. M.; Dorkin, J. R.; Mitchell, M. J.; Fenton, O. S.; Jaklenec, A.; Anderson, D. G.; Langer, R.; Blankschtein, D. Lipid Nanoparticle Assisted mRNA Delivery for Potent Cancer Immunotherapy. *Nano Lett.* **2017**, *17* (3), 1326–1335.

- (60) Riley, R. S.; Kashyap, M. V.; Billingsley, M. M.; White, B.; Alameh, M. G.; Bose, S. K.; Zoltick, P. W.; Li, H.; Zhang, R.; Cheng, A. Y.; Weissman, D.; Peranteau, W. H.; Mitchell, M. J. Ionizable lipid nanoparticles for in utero mRNA delivery. *Sci. Adv.* **2021**, *7* (3), No. eaba1028.
- (61) Cheng, Q.; Wei, T.; Farbiak, L.; Johnson, L. T.; Dilliard, S. A.; Siegwart, D. J. Selective organ targeting (SORT) nanoparticles for tissue-specific mRNA delivery and CRISPR-Cas gene editing. *Nat. Nanotechnol.* **2020**, *15* (4), 313–320.
- (62) Whitehead, K. A.; Dorkin, J. R.; Vegas, A. J.; Chang, P. H.; Veiseh, O.; Matthews, J.; Fenton, O. S.; Zhang, Y.; Olejnik, K. T.; Yesilyurt, V.; Chen, D.; Barros, S.; Klebanov, B.; Novobrantseva, T.; Langer, R.; Anderson, D. G. Degradable lipid nanoparticles with predictable in vivo siRNA delivery activity. *Nat. Commun.* **2014**, *5*, 4277.
- (63) Hajj, K. A.; Ball, R. L.; Deluty, S. B.; Singh, S. R.; Strelkova, D.; Knapp, C. M.; Whitehead, K. A. Branched-Tail Lipid Nanoparticles Potently Deliver mRNA In Vivo due to Enhanced Ionization at Endosomal pH. *Small* **2019**, *15* (6), No. e1805097.
- (64) Jayaraman, M.; Ansell, S. M.; Mui, B. L.; Tam, Y. K.; Chen, J.; Du, X.; Butler, D.; Eltepu, L.; Matsuda, S.; Narayanannair, J. K.; Rajeev, K. G.; Hafez, I. M.; Akinc, A.; Maier, M. A.; Tracy, M. A.; Cullis, P. R.; Madden, T. D.; Manoharan, M.; Hope, M. J. Maximizing the potency of siRNA lipid nanoparticles for hepatic gene silencing in vivo. *Angew. Chem., Int. Ed. Engl.* **2012**, *51* (34), 8529–8533.
- (65) Pardi, N.; Tuyishime, S.; Muramatsu, H.; Kariko, K.; Mui, B. L.; Tam, Y. K.; Madden, T. D.; Hope, M. J.; Weissman, D. Expression kinetics of nucleoside-modified mRNA delivered in lipid nanoparticles to mice by various routes. *J. Controlled Release* **2015**, *217*, 345–351.
- (66) Svitkin, Y. V.; Cheng, Y. M.; Chakraborty, T.; Presnyak, V.; John, M.; Sonenberg, N. N1-methyl-pseudouridine in mRNA enhances translation through eIF2 $\alpha$ -dependent and independent mechanisms by increasing ribosome density. *Nucleic Acids Res.* **2017**, *45* (10), 6023–6036.
- (67) Sahin, U.; Kariko, K.; Tureci, O. mRNA-based therapeutics—developing a new class of drugs. *Nat. Rev. Drug Discov* **2014**, *13* (10), 759–780.
- (68) Kariko, K.; Buckstein, M.; Ni, H.; Weissman, D. Suppression of RNA recognition by Toll-like receptors: the impact of nucleoside modification and the evolutionary origin of RNA. *Immunity* **2005**, *23* (2), 165–175.
- (69) Kauffman, K. J.; Dorkin, J. R.; Yang, J. H.; Heartlein, M. W.; DeRosa, F.; Mir, F. F.; Fenton, O. S.; Anderson, D. G. Optimization of Lipid Nanoparticle Formulations for mRNA Delivery in Vivo with Fractional Factorial and Definitive Screening Designs. *Nano Lett.* **2015**, *15* (11), 7300–7306.
- (70) Ma, F.; Yang, L.; Sun, Z.; Chen, J.; Rui, X.; Glass, Z.; Xu, Q. Neurotransmitter-derived lipidoids (NT-lipidoids) for enhanced brain delivery through intravenous injection. *Sci. Adv.* **2020**, *6* (30), No. eabb4429.
- (71) Hu, Q.; Qian, C.; Sun, W.; Wang, J.; Chen, Z.; Bomba, H. N.; Xin, H.; Shen, Q.; Gu, Z. Engineered Nanoplatelets for Enhanced Treatment of Multiple Myeloma and Thrombus. *Adv. Mater.* **2016**, *28* (43), 9573–9580.
- (72) Lv, F. J.; Tuan, R. S.; Cheung, K.; Leung, V. Concise review: the surface markers and identity of human mesenchymal stem cells. *Stem Cells* **2014**, *32* (6), 1408–1419.
- (73) Florey. The endothelial cell. *Br. Med. J.* **1966**, *2* (5512), 487–90.
- (74) Keller, S.; Nickel, J.; Zhang, J. L.; Sebald, W.; Mueller, T. D. Molecular recognition of BMP-2 and BMP receptor IA. *Nat. Struct. Mol. Biol.* **2004**, *11* (5), 481–8.
- (75) Li, C.; Vepari, C.; Jin, H. J.; Kim, H. J.; Kaplan, D. L. Electrospun silk-BMP-2 scaffolds for bone tissue engineering. *Biomaterials* **2006**, *27* (16), 3115–24.
- (76) Tian, Z.; Wu, L.; Yu, C.; Chen, Y.; Xu, Z.; Bado, I.; Loreda, A.; Wang, L.; Wang, H.; Wu, K.-L.; Zhang, W.; Zhang, X. H.-F.; Xiao, H. Harnessing the power of antibodies to fight bone metastasis. *Sci. Adv.* **2021**, *7* (26), No. eabf2051.
- (77) Kim, Y.-H.; Yang, X.; Shi, L.; Lanham, S. A.; Hilborn, J.; Oreffo, R. O. C.; Ossipov, D.; Dawson, J. I. Bisphosphonate nanoclay edge-site interactions facilitate hydrogel self-assembly and sustains growth factor localization. *Nat. Commun.* **2020**, *11*, 1365.
- (78) Giger, E.; Puigmartí-Luis, J.; Schlatter, R.; Castagner, B.; Dittrich, P.; Leroux, J. Gene delivery with bisphosphonate-stabilized calcium phosphate nanoparticles. *J. Controlled Release* **2011**, *150* (1), 87–93.
- (79) Harper, R.; Fung, B. Resolution of bisphosphonate-associated osteonecrosis of the mandible: possible application for intermittent low-dose parathyroid hormone [rhPTH(1–34)]. *J. Oral. Maxillofac. Surg* **2007**, *65* (5), 573–580.
- (80) De La Vega, R. E.; van Griensven, M.; Zhang, W.; Coenen, M. J.; Nagelli, C. V.; Panos, J. A.; Peniche Silva, C. J.; Geiger, J.; Plank, C.; Evans, C. H.; Balmayor, E. R. Efficient healing of large osseous segmental defects using optimized chemically modified messenger RNA encoding BMP-2. *Sci. Adv.* **2022**, *8* (7), No. eabl6242.